LANGMUIR © Cite This: Langmuir 2019, 35, 2925–2933

Kinetics and Mechanism of Aspartic Acid Adsorption and Its Explosive Decomposition on Cu(100)

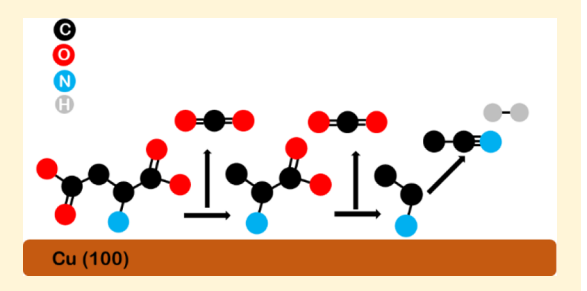
Burcu Karagoz, * Aaron Reinicker, * and Andrew J. Gellman*, *, * to

Department of Chemical Engineering, Carnegie Mellon University, 5000 Forbes Avenue, Pittsburgh, Pennsylvania 15213, United States

*W.E. Scott Institute for Energy Innovation, 5000 Forbes Avenue, Pittsburgh, Pennsylvania 15213, United States

Supporting Information

ABSTRACT: The mechanism and kinetics of aspartic acid (Asp, HO₂CCH(NH₂)CH₂CO₂H) decomposition on Cu(100) have been studied using X-ray photoemission spectroscopy and temperatureprogrammed reaction spectroscopy. We investigate the Asp decomposition mechanism in detail using unlabeled D-Asp and isotopically labeled L-Asp-4-13C (HO₂CCH(NH₂)CH₂13CO₂H), L-Asp-d₇ $(DO_2CCD(ND_2)CD_2CO_2D)$, L-Asp-2,3,3- d_3 $(HO_2CCD(NH_2) CD_2CO_2H$), and L-Asp-¹⁵N-2,3,3- d_3 (HO₂CCD(¹⁵NH₂)CD₂CO₂H). The monolayer of Asp adsorbed on the Cu(100) surface is in a doubly deprotonated bi-aspartate form (-O₂CCH(NH₂)CH₂CO₂-). During



heating, Asp decomposes on Cu(100) with kinetics consistent with a vacancy-mediated explosion mechanism. The mechanistic steps yield CO₂ by sequential cleavage of the C3-C4 and C1-C2 bonds, and N≡CCH₃ and H₂ via decomposition of the remaining CH(NH₂)CH₂ intermediate. Deuterium labeling has been used to demonstrate that scrambling of H(D) occurs during the decomposition to acetonitrile of the CD(NH₂)CD₂ intermediate formed by decarboxylation of L-Asp-2,3,3-d₃ and L-Asp- 15 N-2,3,3- d_3 .

INTRODUCTION

Chirality or "dissymmetry" is the geometric property of objects and molecules that are nonsuperimposable on their mirror images. Molecular chirality is significant because many pharmaceuticals are chiral compounds having two enantiomeric forms. Because of the biomolecular homochirality of living systems, the two enantiomers of chiral pharmaceuticals have very different physiological impacts once ingested.²⁻⁴ This difference mandates the production of enantiomerically pure chiral pharmaceuticals via development of enantioselective chemical processes such as catalysis and separations. Surface chemistry can be enantioselective, if the surfaces have chiral structures⁵⁻⁷ and thus, surface chirality offers an opportunity for the development of new heterogeneous enantioselective chemical processes.

The study of chiral surface chemistry aims to understand the origin of enantiospecific interactions between chiral molecules and chiral surfaces, a challenging goal because the enantiospecific differences in the energetics of such interactions are only a few kJ/mol. The key to understanding the origin of enantioselectivity on chiral surfaces is the determination of surface reaction mechanisms and, in particular, the identification of the specific elementary steps that impart enantioselectivity to the overall mechanism.⁸⁻¹⁰ Understanding reaction mechanisms and kinetics of chiral adsorbates on achiral surfaces can provide insights into the mechanisms and kinetics of surface reactions occurring on chiral surfaces with more complex structures. 11 Herein, we

discuss the surface chemistry of aspartic acid (Asp, HO₂CCH-(NH₂)CH₂CO₂H, Figure 1) on the achiral Cu(100) surface.

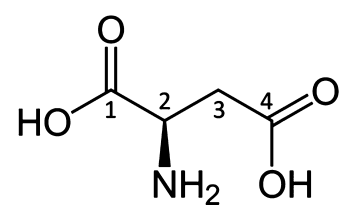


Figure 1. Molecular structure of Asp with carbon atoms labeled.

The simplicity of the Cu(100) surface structure simplifies our analysis of the Asp reaction mechanism and kinetics relative to those on chiral surfaces but, there are many common features between Asp reaction mechanisms on chiral and achiral Cu surfaces. $^{10,12-16}$

Amino acids have attracted attention in surface science because they are among the simplest chiral molecules available for study.¹⁷ In nature, one finds only L-amino acids and, therefore, most studies have been focused on L-amino acids. This work takes advantage of the unique feature that, because they are of biological importance, the L-amino acids are also available in multiple isotopically labeled, enantiomerically pure

Received: October 17, 2018 Revised: January 18, 2019 Published: January 25, 2019

forms. Isotopically labeled L-amino acids allow the study of surface reaction mechanisms and the use of mass spectrometry to identify the structural origins of decomposition fragments desorbing from surfaces. ^{10,13-15,18,19}

The decomposition mechanism of Asp on chiral Cu(643)^{R&S} and achiral Cu(110) surfaces has been studied recently. 10,16,19 Amino acid monomers such as Asp exist in one of three possible chemical forms: neutral (HO2CCH(NH2)- CH_2CO_2H), zwitterionic ($^-O_2CCH(NH_3^+)CH_2CO_2H$), or anionic (-O₂CCH(NH₂)CH₂CO₂H). Because it has two carboxylate groups, Asp can also exist as a di-anion (-O₂CCH(NH₂)CH₂CO₂-). Asp adsorbed on Cu(110) at 400 K exists in this doubly deprotonated, di-anionic form. 10 During decomposition of Asp on Cu(110), the C3-C4 bond breaks first to yield CO₂ in the gas phase, followed by C1-C2 bond cleavage to yield another CO_2 , and finally the remaining CH(NH₂)CH₂ fragment dehydrogenates to acetonitrile (N≡ CCH₃) and H₂ which desorb from the surface. 10,19 Asp dosed from an electrospray ionization source onto the Cu(110) surface undergoes deprotonation at low coverages but, as the coverage increases, Asp is adsorbed on Cu(110) in its zwitterionic or neutral form. ¹⁶ In this work, we use isotopic labeling to gain insight into the kinetics and mechanism of Asp decomposition on the Cu(100) surface and focus particularly on the mechanism of the final dehydrogenation of CH(NH₂)- CH_2 to yield $N \equiv CCH_3$ and H_2 .

On Cu surfaces, Asp and the structurally related compound tartaric acid (TA, HO₂CCH(OH)CH(OH)CO₂H) both decompose via a vacancy-mediated surface explosion mechanism with nonlinear kinetics that yield enantiospecific reaction rates differing by as much as 50× on chiral surfaces such as $Cu(643)^{R\&S}$, $Cu(531)^{R\&S}$ and $Cu(17,5,1)^{R\&S}$. 10,12,20,21 A "surface explosion" is a reaction mechanism that results in an autocatalytic increase in the reaction rate with increasing extent of reaction, even under isothermal conditions. Such vacancymediated explosions were first observed by Madix et al. while studying the decomposition of formic acid on Ni(110).²²⁻² The proposed mechanism is one in which the decomposition of an adsorbate on one site requires an adjacent empty site (vacancy), but the rapid desorption of the decomposition products then leaves two empty sites. These two vacancies then catalyze the decomposition of two adsorbates, yielding four vacancies; hence, there is an auto-catalytic explosion in the vacancy coverage. The first observations of a surface explosion mechanism for a chiral adsorbate were for TA decomposition on the Cu(110) surface. ^{21,25} Later, Mhatre et al. described the explosive surface reaction kinetics of TA/Cu(110) using a rate law which includes an initiation step with rate constant, k_i , and an explosion step with rate constant, $k_{\rm e}$. 20

$$r = -\frac{\mathrm{d}\theta}{\mathrm{d}t} = k_{\mathrm{i}}\theta + k_{\mathrm{e}}\theta(1-\theta)^{2} \tag{1}$$

When the adsorbate coverage is high, $\theta \approx 1$, the initiation step dominates the overall rate; however, once the vacancy concentration, $(1-\theta)$, becomes significant, the explosion step becomes dominant. In the mathematical description of vacancy-mediated explosion kinetics, the "vacancy" is taken in a Langmuirian sense to be a site on the surface that is equivalent to that occupied by the adsorbate, but empty. The literature on these reactions does not try to address the details of how this understanding of site maps onto the physical structure of the surface itself; that is, it does not try to equate a site with a given number and configuration of surface atoms.

The rate expression that best describes the TA decomposition kinetics on Cu(110) is second-order with respect to $(1-\theta)$, suggesting that TA decomposition requires two adjacent vacancies. This is consistent with our observations for Asp decomposition on Cu(100).

This work addresses two of the key challenges in understanding chiral surface chemistry: reaction mechanism and reaction kinetics. Herein, we probe the decomposition mechanism of Asp on Cu(100) using selective 13 C, deuterium (2 H), and 15 N labeling. We demonstrate that Asp decomposes on Cu(100) via a vacancy-mediated explosion mechanism. This is consistent with the high enantiospecificity of D- and L-Asp decomposition on Cu(643)^R&S surfaces. 19 Once the explosive decomposition reaction is initiated, the C3–C4 and C1–C2 bonds break sequentially to produce gas phase CO2. The remaining $-CH(NH_2)CH_2-$ intermediate decomposes into $N \equiv CCH_3$ and H_2 . Using deuterium and $^{15}N_1$ -labeled Asp, we show that hydrogen atoms in the $-CH_1$ -(NH2)CH2- intermediate species are scrambled among the products.

EXPERIMENTAL SECTION

All experiments were performed in a stainless steel ultrahigh vacuum (UHV) chamber with a base pressure $<10^{-9}$ Torr. The UHV chamber is equipped with a $xyz-\varphi$ sample manipulator to move the Cu(100) single crystal sample within the chamber while also allowing heating and cooling over the range T=80-1000 K. The UHV chamber is equipped with: an ion gauge to measure the pressure; an ion gun for Ar⁺ sputter cleaning the Cu(100) surface; a low-energy electron diffraction (LEED) optics to verify the orientation of the clean Cu(100) surface; heated glass evaporators to deposit Asp vapor onto the Cu(100) surface; and a quadrupole mass spectrometer to identify chemical species in the gas phase and to measure product desorption rates during Asp decomposition.

The Cu(100) single crystal sample was 2 mm thick and \sim 10 mm in diameter. The crystal temperature was measured by a K-type thermocouple spot-welded to its edge via thin Ni foil. For each cleaning cycle, the Cu(100) sample was sputtered (\sim 11 μ A of Ar⁺ ions at 1 keV) for 30 min at 750 K in a background pressure of $P_{\rm Ar} \approx$ 7×10^{-5} Torr. The sample was then annealed at 900 K for 10 min before starting the experiment. The orientation of the clean Cu(100) surface was determined by LEED. Then, Asp vapor was deposited onto the Cu(100) surface at 405 K from a glass vial heated to 460 K. The sublimation source was equipped with a shutter to control the exposure time of the Cu(100) surface to Asp. Temperatureprogrammed reaction spectroscopy (TPRS) was performed by placing the crystal ~2 mm away from the circular aperture of the mass spectrometer and heating the surface at a constant rate, while monitoring the signals at m/z ratios corresponding to the expected fragmentation patterns of Asp decomposition products. Isothermal TPRS experiments were conducted by heating the sample at 1 K/s to the desired temperature and then holding the sample at that desired temperature while monitoring product desorption from the surface as a function of time at the isothermal temperature.

Crystalline powders of isotopically labeled L-Asp-4- 13 C (HO₂CCH(NH₂)CH₂ 13 CO₂H, Sigma-Aldrich, 99 atom% 13 C), L-Asp- d_7 (DO₂CCD(ND₂)CD₂CO₂D, Sigma-Aldrich, 98 atom % D), L-Asp-2,3,3- d_3 (HO₂CCD(NH₂)CD₂CO₂H, Cambridge Isotope Laboratories, Inc., 98 atom % D), and L-Asp- 15 N-2,3,3- d_3 (HO₂CCD(15 NH₂)-CD₂CO₂H, Sigma-Aldrich, 98 atom % D, 98 atom % 15 N) were used as received.

Acetonitrile (N \equiv CCH₃, Thermo Scientific, 99.9% purity) and acetonitrile- d_3 (N \equiv CCD₃, Cambridge Isotope Laboratories, Inc., 99.8% purity) were used to determine the pure compound fragmentation patterns in our mass spectrometer. N \equiv CCH₃ (N \equiv CCD₃) was first transferred to a clean glass vial and treated with multiple freeze–pump–thaw cycles to remove high vapor pressure

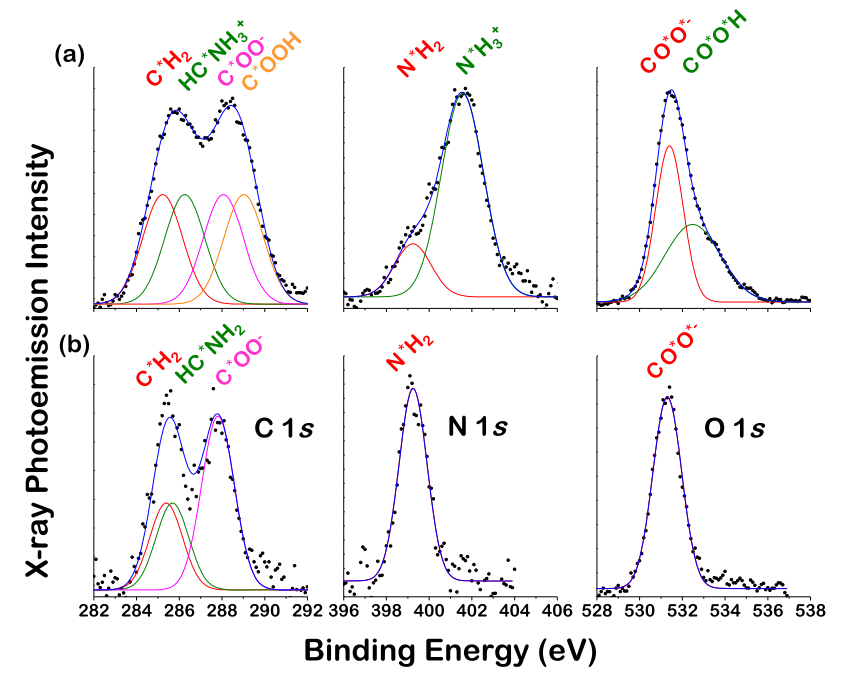


Figure 2. C 1s, N 1s, and O 1s XPS spectra from D-Asp on Cu(100). (a) D-Asp multilayer on Cu(100). The C 1s feature of C*OOH, N 1s feature of N*H₃⁺, and the O 1s feature of CO*O*H all indicate that the D-Asp multilayer is zwitterionic. (b) D-Asp monolayer on Cu(100). The absence of the C*OOH, N*H₃⁺, and CO*O*H peaks indicates that in the monolayer D-Asp adsorbs as biaspartate, $-O_2CCH(NH_2)CH_2CO_2-$.

impurities before introducing vapor into the chamber using a leak valve. Mass spectra of both $N \equiv CCH_3$ and $N \equiv CCD_3$ were collected at 5×10^{-8} Torr for m/z = 38-44 before each set of L-Asp TPRS experiments. For each spectrum, the signal intensities at all m/z = 38-44 were normalized to signals at m/z = 38 (NCC^+).

X-ray photoemission spectroscopy (XPS) was performed in a Thermo Fisher Theta Probe operated at a base pressure of 10^{-9} Torr. XPS spectra were taken with the sample at room temperature using a 400 μ m X-ray spot size and a 40 eV analyzer pass energy. The Cu(100) surface was cleaned by two cycles of sputtering and annealing. The surface at 700 K was sputtered with 2 keV Ar⁺ ions with a sputtering current of 10 μ A for 40 min and annealed at 750–800 K for >10 min. XPS was performed at five points on the Cu(100) surface to determine whether the surface was clean. The surface was then exposed at 330 K to Asp vapor to adsorb a multilayer of Asp. After obtaining an XPS spectrum of multilayer Asp, the surface was heated to 405 K to obtain a monolayer of Asp on the surface before its XPS spectrum was acquired.

■ RESULTS AND DISCUSSION

Chemical State of D-Asp/Cu(100). XPS has been used to determine the chemical state of Asp on Cu(100). 10,16 We performed an XPS analysis of D-Asp multilayers and monolayers adsorbed on the Cu(100) surface. To produce a multilayer of D-Asp on the surface, the Cu(100) surface was exposed to D-Asp for 1 h with the sample held at T < 330 K. Figure 2a shows the C 1s, N 1s, and O 1s XPS spectra for a multilayer of D-Asp on the Cu(100) surface. An asterisk (*) indicates the atom in each of the chemical groups that is probed by each XPS spectrum. To estimate the contributions to the spectra from the different chemical groups in D-Asp/ Cu(100), we used the multiple peak analyzer tool in OriginPro and a Gaussian peak fitting function. The broad C 1s XPS spectrum has been fit by four peaks with binding energies of 285.2 eV for C*H₂, 286.3 eV for HC*NH₃⁺, 288.1 eV for C*OO⁻, and 289.0 eV for C*OOH. 10,26-31 The four peaks used to fit the C 1s multilayer spectrum have been constrained

to have identical widths and areas while the energies were allowed to vary. For N 1s, there are peaks at binding energies of 401.6 eV for N*H $_3$ ⁺ and 399.2 eV for N*H $_2$. $^{10,16,26-35}$ The areas of these two peaks suggests that the ratio of Asp in the zwitterionic multilayer to Asp in the biaspartate monolayer is \sim 4. The two peaks used to fit the multilayer N 1s spectrum have the same width. For O 1s, there are peaks at binding energies of 531.4 eV for CO*O* and 532.5 eV for CO*O*H. $^{10,16,26-36}$ The two peaks used to fit the multilayer O 1s spectrum have identical area. These XPS spectra indicate that at multilayer coverages, the D-Asp species on the surface is zwitterionic ($^{-}$ O₂CCH(NH $_3$ ⁺)CH $_2$ CO $_2$ H).

A monolayer of D-Asp on the Cu(100) surface was created by heating the D-Asp multilayer on the Cu(100) surface to 405 K for ~10 min. Figure 2b shows C 1s, N 1s, and O 1s XPS spectra for a monolayer of D-Asp on the Cu(100) surface. The C 1s spectrum now contains three peaks at: 285.4 eV for C*H₂, 285.7 eV for HC*NH₂, and 287.9 eV for C*OO^{-.10,26-31} The three peaks used to fit the C 1s monolayer spectrum have the same widths. The peaks for the C*H₂ and HC*NH₂ groups have equal areas while the single peak for the C*OO groups has twice that area. The binding energy was allowed to vary. The peaks for C*H2 and HC*NH2 are not resolvable in the spectrum and therefore not strictly assignable. We have used two peaks to represent this region of the spectrum based on the assumption that there are two different C atoms in the range of binding energies around 285.5 eV. The peak for C*OOH that was present at 288.9 eV in the multilayer clearly disappears in the C 1s spectrum of the monolayer. The N 1s spectrum contains only one peak at 399.2 eV assigned to N*H₂, and the O 1s spectrum also contains only one peak at a binding energy of 531.3 eV which is assigned to CO*O*-. 10,16,26-36 The peaks for CO*O*H and N*H₃⁺ observed in the multilayer spectrum have disappeared in the spectrum of the monolayer. These changes in the XPS spectra demonstrate that the D-Asp monolayer species is bi-

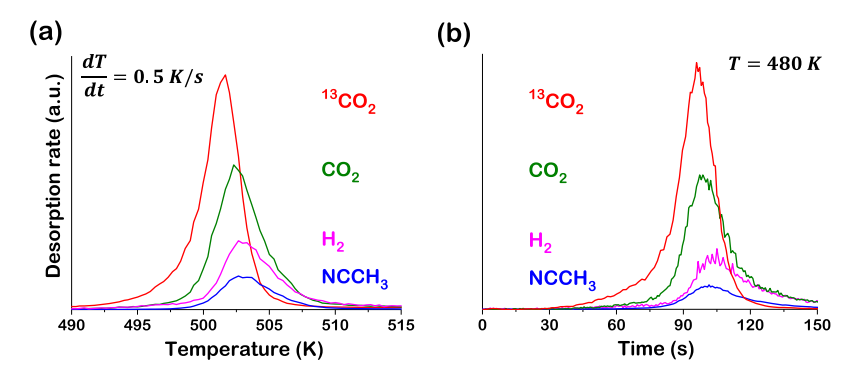


Figure 3. TPRS spectra of L-Asp-4- 13 C decomposition on Cu(100). (a) TPRS at a heating rate of 0.5 K/s. (b) Isothermal TPRS at 480 K. The signals for m/z = 2 (H₂), 41 (N \equiv CCH₃), 44 (CO₂), and 45 (13 CO₂) were collected. Initially, L-Asp-4- 13 C is adsorbed on the surface as biaspartate ($-O_2$ CCH(NH₂)CH₂ 13 CO₂-). The C3-C4 and C1-C2 bonds break sequentially yielding 13 CO₂ and CO₂, respectively. The remaining CH(NH₂)CH₂ intermediate then decomposes to produce N \equiv CCH₃ and H₂.

aspartate ($-O_2CCH(NH_2)CH_2CO_2-$). XPS results agree well with a previous study of L-Asp adsorbed on Cu(110) which also demonstrates that in a multilayer film, L-Asp adsorbs as a zwitterion ($^-O_2CCH(NH_3^+)CH_2CO_2H$) while at monolayer coverage, L-Asp is a doubly deprotonated ($^-O_2CCH(NH_2)-CH_2CO_2-$) di-anion in which both carboxylate groups interact with the Cu surface. Using both XPS and PM-RAIRS, Totani et al. also showed that deprotonation of the COOH groups in Asp occurs at low coverages on Cu(110), but as the coverage increases, NH_3^+ groups indicative of the zwitterion are observed. Groups in the coverage increases, NH_3^+ groups indicative of the zwitterion are observed.

Decomposition of 13 C-Labeled L-Asp/Cu(100). The use of isotopically labelled L-amino acids on surfaces enables the decomposition mechanism to be probed during heating. Initially, the Cu(100) surface at 405 K was saturated with L-Asp-4-13C. This leads to the formation of bi-aspartate, as demonstrated in Figure 2, and desorption of H2 (not detected during adsorption). The TPRS spectra in Figure 3 provide insight into the sequence of steps by which L-Asp-4-13C/ Cu(100) decomposes. We obtained TPRS spectra while monitoring the desorption signals at m/z = 2 (H₂), 41 (N= CCH₃), 44 (CO₂), and 45 (¹³CO₂). While heating the surface saturated with L-Asp-4-13C at 0.5 K/s (Figure 3a), the C3-C4 bond breaks first, releasing labeled 13CO2 which desorbs rapidly from the surface at T = 501.6 K. The cleavage of the C1–C2 bond occurs at slightly higher temperature ($\Delta T = 0.7$ \pm 0.1 K), yielding unlabeled CO₂ which desorbs at T = 502.3K. Finally, the CH(NH₂)CH₂ species left on the surface decomposes to produce $N \equiv CCH_3$ and H_2 which desorb at T = 503.1 K. Figure 3b shows the rates of product desorption during isothermal heating of the L-Asp-4-13C-saturated Cu-(100) surface at 480 K. This reveals the same sequence of decomposition steps as observed during heating the surface at a constant rate. Isothermal decomposition of L-Asp-4-13C on Cu(100) begins after a ~30 s induction period. The rate of ¹³CO₂ desorption reaches a maximum at ~96 s, while the desorption rate of unlabeled CO₂ reaches a maximum at ~99 s. This shows that the C3-C4 bond breaks before the C1-C2 bond. The maximum rates of N≡CCH3 and H2 desorption occur at ~102 and 104 s, respectively, as a result of the decomposition of the CH(NH₂)CH₂ intermediate generated by double decarboxylation of the adsorbed Asp.

The XPS and TPRS results are consistent with the mechanism below which starts with the formation of biaspartate during adsorption at 405 K followed by a sequence of decomposition steps.

$$\begin{split} & H - O_2 CCH(NH_2) CH_2^{13} CO_2 - H_{(g)} \\ & \stackrel{k_{ads}}{\longrightarrow} O_2 CCH(NH_2) CH_2^{13} CO_2 + H_{2(g)} \\ & O_2 CCH(NH_2) CH_2 - {}^{13} CO_2 \\ & \stackrel{k_1}{\longrightarrow} O_2 CCH(NH_2) CH_2 + {}^{13} CO_2(g) \\ & O_2 C - CH(NH_2) CH_2 \stackrel{k_2}{\longrightarrow} CH_2 CH(NH_2) + CO_{2(g)} \\ & CH_2 CH(NH_2) \stackrel{k_3}{\longrightarrow} N \equiv CCH_{3(g)} + H_{2(g)} \end{split}$$

The decomposition of Asp on Cu surfaces seems to progress quite cleanly to yield CO_2 , H_2 , and $N \equiv CCH_3$. A recent molecular beam study shows that on Cu(111) the reaction can continue in the steady state to >40 turnovers without apparent contamination and deactivation of the surface. Whether this is true of all surfaces is not clear.

TPRS and XPS experiments have enabled us to identify the products and the mechanism of L-Asp decomposition on Cu(100). Using isotopomers of L-Asp on Cu(110), Mhatre et al. also demonstrated that the C3–C4 bond breaks first to yield CO_2 , and then the C1–C2 bond breaks yielding another CO_2 and a $CH(NH_2)CH_2$ species that decomposes into H_2 and $N \equiv CCH_3$.

H(D) Isotope Distribution in Acetonitrile from Partially Deuterated L-Asp/Cu(100). The use of ¹³C-labeled L-Asp reveals that the order of C-C bond cleavage is the same on Cu(100) as previously observed on Cu(110). However, the decomposition mechanism of the CH(NH₂)CH₂ fragment that remains after decarboxylation of Asp is not clear. The structure of the intermediate is not known but we assume that it starts as CH(NH₂)CH₂, analogous to the species that would be produced by adsorption of ethyleneamine. We address the mechanistic question of which two hydrogen atoms end up in the gas phase as H₂ by using L-Asp-d₇ (DO₂CCD(ND₂)- CD_2CO_2D), L-Asp-2,3,3- d_3 (HO₂CCD(NH₂)CD₂CO₂H), and L-Asp-15N-2,3,3-d₃ (HO₂CCD(15NH₂)CD₂CO₂H) and determining the deuterium distribution in the acetonitrile produced by each isotopomer. The formation of N≡CCH₃ from CH(NH₂)CH₂ requires dissociation of the two N-H bonds, dissociation of the secondary C-H bond, and formation of a primary C-H bond to form the methyl group. This presumably requires hydrogen transfer to and from the surface or perhaps between adsorbed intermediates. The question is

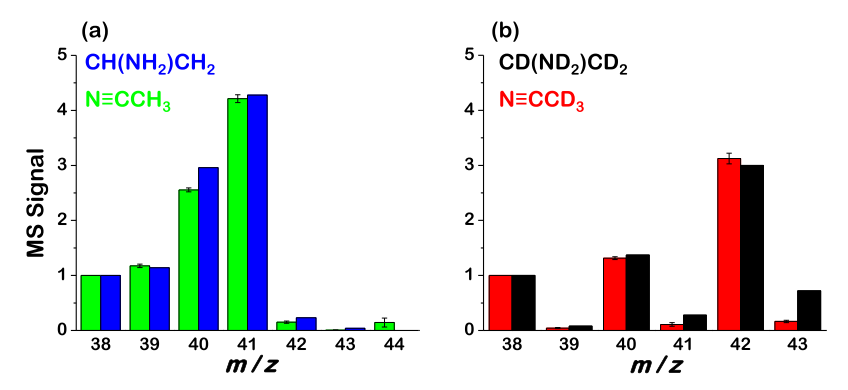


Figure 4. Fragmentation patterns of (a) $N \equiv CCH_3$ (green) and (b) $N \equiv CCD_3$ (red) and the fragmentation patterns of acetonitrile generated by decomposition of (a) L-Asp-4- ^{13}C (blue) and (b) L-Asp- d_7 (black) on Cu(100). The fragmentation patterns of $N \equiv CCH_3$ and $N \equiv CCD_3$ were obtained by introducing their vapors into the chamber. The fragmentation patterns of acetonitrile produced during decomposition of $CH(NH_2)CH_2$ and $CD(ND_2)CD_2$ were calculated from the areas under the TPRS spectra of L-Asp-d- ^{13}C and L-Asp-d- 7 . The signal intensities are all normalized to that of the lowest m/z = 38 fragment ($N \equiv CC^+$).

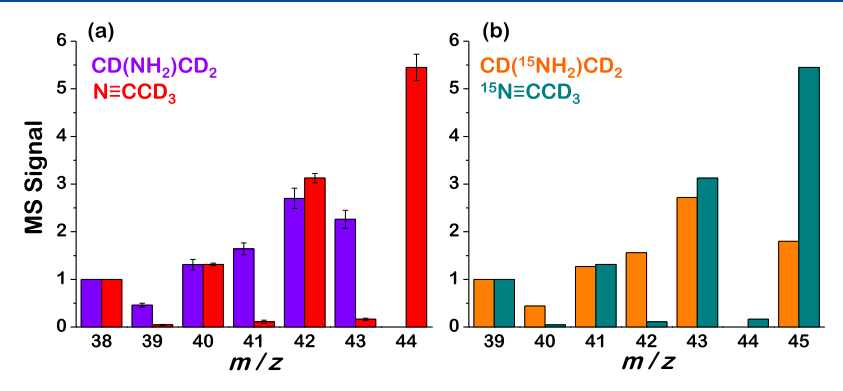


Figure 5. Fragmentation patterns of acetonitrile desorbed from the surface during decomposition of (a) L-Asp-2,3,3- d_3 (purple bars) and (b) L-Asp- 15 N-2,3,3- d_3 (orange bars) on Cu(100). The fragmentation patterns were calculated from areas under the TPRS spectra and normalized to the signals at m/z = 38 (L-Asp- 2 3,3- d_3) and m/z = 39 (L-Asp- 15 N-2,3,3- d_3). Comparison to the fragmentation patterns for N=CCD₃ and the expected fragmentation pattern for 15 N=CCD₃ reveal poor correspondence. Fragmentation at m/z = 44 is ignored for CD(NH₂)CD₂ and CD(15 NH₂)CD₂ decomposition.

whether there is scrambling of the hydrogen atoms in the process through multiple C–H and N–H dissociation and recombination steps. For example, the decomposition of a $CD(NH_2)CD_2$ fragment could result in one single isotopomer of acetonitrile (e.g. $N \equiv CCD_3$ if the H atoms on the $-NH_2$ group form H_2 exclusively) or many isotopomers. The possible decomposition products of the $CD(NH_2)CD_2$ intermediate resulting from L-Asp-2,3,3- d_3 /Cu(100) are

$$CD(NH_2)CD_2 \rightarrow N \equiv CCD_3(N \equiv CCD_2H, N \equiv$$

$$CCDH_2, N \equiv CCH_3) + H_2(HD, D_2)$$

Note that the formation of N \equiv CCH₃ would require the exchange of hydrogen atoms between molecules, perhaps via the surface.^{37–40} Our experiments with L-Asp-4-¹³C, L-Asp- d_{7} , L-Asp-2,3,3- d_{3} , and L-Asp-¹⁵N-2,3,3- d_{3} have been conducted with the goal of determining the distribution of H and D atoms in the product acetonitrile.

To determine the fragmentation patterns of all four possible acetonitrile products, we have obtained the $N \equiv CCH_3$ and $N \equiv CCD_3$ fragmentation patterns by introducing pure $N \equiv CCH_3$ and $N \equiv CCD_3$ vapors into the chamber. The mass spectrometer signal at the lowest m/z = 38 ($N \equiv CC^+$) is scaled to a value of 1 and the signals at other masses (partially hydrogenated $N \equiv CCH_n^+$ ions) are normalized to the m/z = 38 signal. For $N \equiv CCH_3$, the largest signal is observed at m/z

= 41, and the major fragments are observed at m/z = 38, 39, and 40 as a result of H atom loss. For N \equiv CCD₃, the signal at m/z = 44 is maximum and the major fragments of N \equiv CCD₃ ionization are detected at m/z = 38, 40, and 42 because of D loss (Figure 4).

To study the decomposition mechanism of L-Asp on Cu(100), TPRS experiments were performed with both a constant heating rate of 0.5 K/s and isothermally at 480 K using L-Asp-4- $^{1\bar{3}}$ C, L-Asp- d_7 , L-Asp-2,3,3- d_3 , and L-Asp- 15 N-2,3,3-d₃ (Figures S1 and S2). Decarboxylation of these isotopomers, once adsorbed as bi-aspartate, is presumed to lead to the formation of four different intermediates: CH(NH₂)CH₂, CD(ND₂)CD₂, CD(NH₂)CD₂, and CD-(15NH₂)CD₂. By determining the distribution of deuterium atoms in the acetonitrile decomposition products (Figures 4 and 5), we gain insight into the decomposition mechanism of this intermediate. The fragmentation patterns of acetonitrile produced by the decomposition of the intermediate species isotopomers were determined from the areas under the TPRS spectra obtained at m/z = 38 (N \equiv CC⁺), 39 (N \equiv CCH⁺, $^{15}N \equiv CC^{+}$), 40 (N=CCH₂⁺, N=CCD⁺, $^{15}N \equiv CCH^{+}$), 41 (N=CCH₃, N=CCDH⁺, $^{15}N \equiv CCH_2^{+}$, $^{15}N \equiv CCD^{+}$), 42 (N=CCDH₂⁺, N=CCD₂⁺, $^{15}N \equiv CCDH^{+}$), 43 $(N \equiv CCD_2H^+, {}^{15}N \equiv CCDH_2^+, {}^{15}N \equiv CCD_2^+)$, and 45 (${}^{15}N \equiv$ CCD₃). The signals at m/z = 44 were ignored because they coincide with the CO2 signal which overwhelms the

contribution at m/z = 44 from N \equiv CCD₃. The signal intensity at the lowest m/z (38 or 39) from the TPRS spectra of each C₂H_nD_{5-n}N intermediate is assumed to be 1 and the signals at other values of m/z are normalized to that at the lowest m/z. The same normalization procedure was applied to the mass spectra of pure N \equiv CCH₃ and N \equiv CCD₃ vapors.

The acetonitrile isotopomers produced during L-Asp-4-13C and L-Asp- d_7 decomposition on Cu(100) can only be N= CCH₃ and N≡CCD₃, respectively, so first we compare the acetonitrile fragmentation patterns from L-Asp-4-13C and L-Asp- d_7 with those from the pure N \equiv CCH₃ and N \equiv CCD₃ samples (Figure 4). The fragmentation pattern of acetonitrile produced during L-Asp-4-13C decomposition is similar to the fragmentation pattern of N≡CCH3 introduced to the UHV chamber. The largest signal observed during CH(NH₂)CH₂ decomposition is detected at m/z = 41 due to $(N \equiv CCH_3^+)$, and the other major fragments are observed at m/z = 38, 39,and 40. As shown in Figure 4a, the intensities of the signals at m/z = 39, 40, and 41 relative to that at m/z = 38 are almost identical for both N≡CCH₃ (green) and CH(NH₂)CH₂ (blue), indicating that the L-Asp-4-13C decomposition product is indeed N≡CCH₃. During L-Asp-d₇ decomposition, the highest signal is expected at m/z = 44 (N \equiv CCD₃⁺), however, we ignore the m/z = 44 signals because they overlap those from CO2. The largest of the remaining signals observed during L-Asp- d_7 decomposition occur at m/z = 38, 40, and 42 (Figure 4b). The fact that the intensities of the signals from L-Asp- d_7 at m/z = 40 and 42 (black) match those from N CCD₃ (red) demonstrates that N≡CCD₃ is the product of L-Asp- d_7 decomposition on Cu(100).

We use L-Asp-2,3,3- d_3 and L-Asp- 15 N-2,3,3- d_3 TPRS (Figure 5) to determine whether there is more than one acetonitrile isotopomer formed during decomposition of the CD(NH₂)-CD₂ intermediate. During decomposition of L-Asp-2,3,3-d₃ (Figure 5a, purple), the highest intensity desorption signal is observed at m/z = 42 (N \equiv CCD₂⁺ or N \equiv CCH₂D⁺). We also observe a signal at m/z = 41 (N \equiv CCHD⁺ or N \equiv CCH₃⁺). The large m/z = 43 signal corresponds to N=CCD₂H⁺ which can only be produced by the transfer of at least one H atom from the NH₂ group to the CD₂ group. This indicates that there is a scrambling of hydrogen atoms within the adsorbed CD(NH₂)CD₂ intermediate during its decomposition. Because we ignore the m/z = 44 signal which might be the possible acetonitrile product N≡CCD₃⁺, we also performed TPRS experiments using L-Asp- 15 N-2,3,3- d_3 on Cu(100) (Figure 5b, orange bars). ¹⁵N≡CCD₃ is clearly one of the products because it is the only possible fragment with a signal at m/z =45. There is a large signal at m/z = 42 ($^{15}N \equiv CCDH^+$ or 15 N \equiv CCH₃⁺) among the fragments of L-Asp- 15 N-2,3,3- d_3 decomposition. This clearly proves that some of the products acetonitrile isotopomers contain H atoms and that there is scrambling of H(D) atoms during C-H(D) and N-H bond cleavage and formation.

Quantification of H(D) Scrambling in Acetonitrile from L-Asp/Cu(100). This work advances our understanding of the Asp decomposition mechanism on Cu surfaces by probing the fate of the hydrogen atoms in the CH(NH₂)CH₂ intermediate generated by decarboxylation of Asp. The ideal isotopomer for the study of H(D) scrambling in CH(NH₂)-CH₂ on Cu surfaces would be L-Asp-1,4- 13 C₂-2,3,3-d₃. In this compound, the m/z = 44 signal from N \equiv CCD₃⁺ would not coincide with the m/z = 45 signal from 13 CO₂, and we could observe the H and D distribution in the desorbed acetonitrile

products. Unfortunately, L-Asp-1,4- 13 C₂-2,3,3- d_3 is not commercially available. Therefore, we have used commercially available L-Asp- d_7 , L-Asp-N-2,3,3- d_3 , and L-Asp- 15 N-2,3,3- d_3 to obtain fragmentation patterns from the acetonitrile products generated by their decomposition on Cu(100). In doing so, we have ignored signals at m/z=44 that overlap those from CO₂ production.

In order to extract the acetonitrile isotopomer distribution resulting from L-Asp-2,3,3- d_3 and L-Asp- 15 N-2,3,3- d_3 decomposition on Cu(100), we need the fragmentation patterns of all four partially deuterated acetonitrile isotopomers. Not surprisingly, the fragmentation patterns of N \equiv CCH $_3$ and N \equiv CCD $_3$ are almost identical (Figure 6, red and cyan hashed

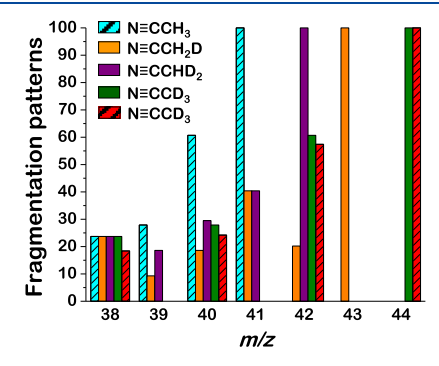


Figure 6. Estimated fragmentation patterns for the three possible deuterated acetonitrile isotopomers: $N \equiv CCH_2D$ (orange), $N \equiv CCD_2H$ (purple), and $N \equiv CCD_3$ (dark green). These have been estimated from the measured fragmentation pattern of $N \equiv CCH_3$ (cyan bars). The hashed bars represent experimentally determined fragmentation patterns for $N \equiv CCH_3$ (cyan) and for $N \equiv CCD_3$ (red).

bars). We have predicted the fragmentation patterns of the deuterated acetonitrile isotopomers based on the experimentally measured fragmentation pattern of N≡CCH₃ (cyan hashed bar). The pattern predicted for $N \equiv CCD_3$ (green bar) is almost identical to the measured fragmentation pattern (red hashed bar). The acetonitrile fragmentation patterns obtained from TPRS of L-Asp-2,3,3- d_3 and L-Asp- 15 N-2,3,3- d_3 decomposition on Cu(100) and shown in Figure 5 differ from those estimated for any single acetonitrile isotopomer. As a result, we conclude that the acetonitrile products from L-Asp must consist of multiple isotopomers arising from H(D) scrambling in the decomposition process. Figure 5b shows that relative to the reference signal at m/z = 39 (15N \equiv CC+), the decomposition of L-Asp-15N-2,3,3-d3 (orange bars) yields much less signal at m/z = 45 than expected for pure ¹⁵N \equiv CCD₃. Similarly, the signal at m/z = 42 must arise from a Hcontaining isotopomer: ¹⁵N≡CCD₂H, ¹⁵N≡CCH₂D or ¹⁵N≡CCH₃ (or some combination thereof). To quantify the isotopomer distribution, we use the equation below to predict the fractional partial pressures of acetonitrile isotopomers.

$$S_{m/z} = \alpha_{d0}^{m/z} f_{d0} + \alpha_{d1}^{m/z} f_{d1} + \alpha_{d2}^{m/z} f_{d2} + \alpha_{d3}^{m/z} f_{d3}$$
 (2)

$$f_{d0} + f_{d1} + f_{d2} + f_{d3} = 1 ag{3}$$

where $S_{m/z}$ is the area under the TPRS curve at a given m/z ratio, $\alpha_{\rm X}^{m/z}$ is the fragmentation fraction for acetonitrile isotopomer dn, where n is the number of D atoms, and f_{dn} is the fractional yield of isotopomer dn. The values of $\alpha_{\rm X}^{m/z}$ are

Table 1. Normalized Fractions of Acetonitrile Isotopomer Generated from the Decomposition of L-Asp Calculated Using the Fragmentation Pattern for Pure $N \equiv CCD_3^a$

	f_{d3}	f_{d2}	f_{d1}	f_{d0}
l-Asp- d_7	1.0(1.0)			
l-Asp- ¹⁵ N-2,3,3-d ₃	0.26(0.33)	0.23(0.38)	0.42(0.24)	0.09(0.05)
l-Asp-2,3,3- d_3 l-Asp-4- 13 C	0.20(0.31)	0.45(0.41)	0.33(0.23)	0.02(0.05) 1.0(1.0)

^aValues in parenthesis are calculated using pure N≡CCD₃ fragmentation pattern.

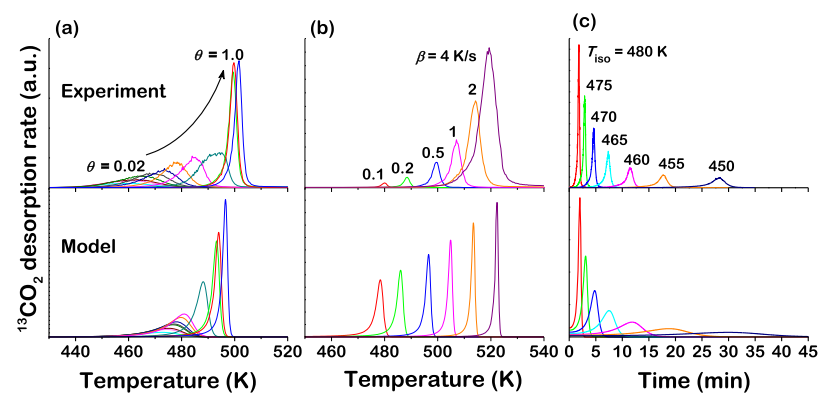


Figure 7. Measured $^{13}\text{CO}_2$ desorption rate during L-Asp-4- 13 C decomposition on Cu(100) (top row): (a) vs temperature at variable initial coverages ($\theta_0 = 0.02-1$), (b) vs temperature at variable heating rates ($\beta = 0.1-4$ K/s) with an initial coverage of $\theta_0 = 1$, and (c) vs time at isothermal temperatures (450–480 K) with an initial coverage of $\theta_0 = 1$. The lower row illustrates simulated TPRS spectra obtained using eq 1 with kinetic parameters obtained by fitting to the experimental data.

estimated from the fragmentation patterns of pure $N \equiv CCH_3$ and $N \equiv CCD_3$ shown in Figure 6.

Table 1 exhibits calculated normalized fractions of acetonitrile produced during L-Asp isotopomer decomposition on Cu(100). During L-Asp- d_7 decomposition, the only possible acetonitrile product is $N \equiv CCD_3$ and during L-Asp-4- ^{13}C decomposition $N \equiv CCH_3$ is the only possible product. During L-Asp- ^{15}N -2,3,3- d_3 decomposition on Cu(100), we observe desorption of all four acetonitrile isotopomers. Not too surprisingly, the yields of $N \equiv CCH_3$ are low because its production requires intermolecular H transfer. This suggests that the $CD(NH_2)CD_2$ decomposition yields acetonitrile predominantly by intramolecular H(D) transfer processes. These data clearly reveal that there is scrambling of H and D atoms within the $CD(NH_2)CD_2$ fragments generated by decarboxylation of the deprotonated Asp.

L-Asp/Cu(100) Decomposition Kinetics. The decomposition kinetics of L-Asp on Cu(100) exhibit characteristics of a vacancy-mediated explosion mechanism. 12,20,22-24 The upper row of Figure 7 shows the decomposition kinetics of L-Asp-4-13C on Cu(100) measured by TPRS using variable initial coverages, variable heating rates at saturation coverage, and variable isothermal temperatures at saturation coverage. The signals monitor the desorption of ${}^{13}CO_2$ at m/z = 45. The lower row of Figure 7 shows spectra predicted by a kinetic model (eq 1) parameterized by fitting to the experimental data. Figure 7a shows the ¹³CO₂ desorption rate measured at a constant heating rate of 0.5 K/s for initial coverages of L-Asp-4-13C spanning the range $\theta_0 = 0.02-1$. At low coverages, the peak $^{13}CO_2$ desorption temperature decreases from $T_p = 474$ 458 K over the coverage range $0.02 \le \theta \le 0.22$ (Figure S3). However, as θ increases further, the peak temperature begins to increase and reaches a maximum value of 501.7 K at the saturation coverage, $\theta_0 = 1$. In addition, the peak width

decreases as coverage increases from 0.02 to 1. When $\theta_0 \approx 1$ the desorption peak becomes very narrow (FWHM ~3 K). At low Asp coverages, the peaks overlap one another, however, when $\theta > 0.47$, the leading edges begin to undercut those at lower coverages. This indicates a decrease in the initial reaction rate with increasing coverage. In the vacancy-mediated explosion kinetics, this occurs because the fractional coverage of empty sites, $(1 - \theta)$, decreases as the initial coverage increases and approaches zero as the coverage approaches $\theta_0 \approx$ 1. These results are very similar to those observed previously for the decomposition of TA on Cu(110). This is a hallmark of vacancy-mediated explosion kinetics; at high coverages, a slow initiation process creates the vacancies needed for the explosion step. Once the vacancy coverage reaches a critical value, the explosion step generates additional vacancies auto-catalytically leading to acceleration of the reaction rate and completion over a very short time (temperature) interval.

We have also examined the explosive decomposition kinetics of L-Asp-4-¹³C on Cu(100) by performing TPRS experiments with heating rates in the range $\beta = 0.1-4$ K/s (Figure 7b) and at isothermal temperatures varying from $T_{\rm iso}$ = 450 K to 480 K (Figure 7c) at θ_0 = 1. The variable heating rate measurements reveal that T_p increases from 480 to 519 K with increasing heating rate. The isothermal TPRS experiments reveal characteristics that are clear indicators of the vacancy-mediated explosion mechanism. For isothermal TPRS, the Cu(100) sample was heated to the desired temperature at a constant rate of 1 K/s and then held at $T_{\rm iso}$. Initially, the decomposition rate is very low during the initiation phase, and then increases rapidly during the explosion phase. 12,20 Figure 7c shows that at $T_{\rm iso}$ = 450 K, there is an induction period of ~22 min during which no ¹³CO₂ desorption is detected. Then, L-Asp-4-¹³C begins to decompose and the ¹³CO₂ desorption rate reaches a

maximum at ~27 min before dropping back to zero as the Asp monolayer is consumed. As $T_{\rm iso}$ decreases, the initiation period increases. This general behavior of initiation followed by rapidly accelerating decomposition is indicative of vacancy-mediated explosive decomposition of L-Asp-4- 13 C on Cu(100).

The decomposition kinetics of L-Asp on Cu(100) are quite complex. The process clearly reveals features that are characteristic of a vacancy-mediated explosion reaction. By this, we mean that the kinetics of the first step in the reaction, cleavage of the C3-C4 bond, are described by the kinetics of a surface explosion. The spectra in Figure 7 reveal an increase in the peak CO₂ desorption temperatures with increasing coverage, and the isothermal TPRS experiments reveal a long nucleation period before the onset of an accelerating decomposition rate. At high initial coverages, there is a nucleation or initiation process that creates vacancies in the adsorbed monolayer. ^{10,12,20,22-24} These vacancies enable decomposition of adjacent L-Asp via cleavage of the C3-C4 bond followed by cleavage of the C1-C2 bond and decomposition of the remaining CH(NH₂)CH₂ intermediate. TA also decomposes by a vacancy-mediated explosion mechanism on Cu surfaces. In contrast to the L-Asp decomposition products, all the TA decomposition products appear simultaneously indicating that their appearance is rate limited by one common step in the decomposition mechanism. 10,20

The previously suggested rate law for the explosive decomposition of TA/Cu(110) (eq 1) has been used to model the TPRS for L-Asp decomposition on Cu(100) as shown in Figure 7 (top row). At high initial coverages of L-Asp, the initiation step creates vacancies. Once the vacancy coverage reaches a critical value, the surface explosion step causes the rate to accelerate auto-catalytically. The decomposition kinetics of L-Asp on the Cu surface are more complicated than those of TA. During TA decomposition, all fragments desorb simultaneously, suggesting that the rate limiting step is followed by rapid decomposition to products and their desorption.²⁰ As we demonstrate in Figure 3, the initial production of ¹³CO₂ from cleavage of the C3-C4 bond in L-Asp-4-13C slightly precedes the cleavage of the C1-C2 bond to yield CO₂ and the decomposition of the remaining CH(NH₂)CH₂ fragment. For the purposes of modeling the L-Asp-4-13C decomposition rate, r, we have focused on the ¹³CO₂ desorption rate only; that is, the initial decomposition step. The pre-exponential factors (A_i, A_e) and activation energies $(\Delta E_{\rm i}, \Delta E_{\rm e})$ of the initiation rate constant, $k_{\rm i} = A_{\rm i} \, {\rm exp} \Big(- {\Delta E_{\rm i} \over RT} \Big)$, and explosion rate constant $k_{\rm e} = A_{\rm e} \, \exp \left(- \frac{\Delta E_{\rm e}}{RT} \right)$ have been estimated by fitting eq 1 to the data in Figure 7. In these rate constants, R is the gas constant and T is the temperature. The parameter estimation has been done by minimizing the difference between predicted and measured values of peak temperature, T_p , for the TPRS obtained with varying initial coverages and heating rates and the peak time, $t_{\rm p}$, for the TPRS at varying isothermal temperatures (SSE = $\sum (x_{\rm expt} - x_{\rm model})^2/x_{\rm expt}^2$, where x is $T_{\rm p}$ or $t_{\rm p}$). Errors (2σ) in the estimated values are at the 95% confidence interval. The order of the reaction in the vacancy concentration is fixed at n = 2 as was found for TA decomposition on Cu(110).20 As observed in the case of TA decomposition kinetics, attempts to fit the Asp kinetics using values of n = 1 or n = 3 yielded poorer fits than with n = 2. This

implies that L-Asp decomposition on Cu(100) also requires two vacancies. The values of the kinetic parameters that yield the best fits to the data are listed in Table 2.

Table 2. Kinetic Parameters Estimated for the Explosive Decomposition of L-Asp-4-¹³C/Cu(100)

$A_{\rm i}~(\rm s^{-1})$	$\Delta E_{\rm i}$ (kJ/mol)	$A_{\rm e}~(\rm s^{-1})$	$\Delta E_{\rm e}$ (kJ/mol)
$10^{10\pm1}$	119 ± 5	$10^{22\pm1}$	209 ± 8

The bottom row of Figure 7 shows the simulated TPRS generated using the optimum values of the kinetic parameters. The simulated TPRS shows the characteristics of a vacancy-mediated surface explosion: peak temperature increases with increasing coverages, peaks become narrower as coverage increases, and the reaction initiation time increases with decreasing isothermal temperatures.

CONCLUSIONS

At monolayer coverages, Asp adsorbs on Cu(100) at 405 K in the doubly deprotonated bi-aspartate form. In multilayer films adsorbed at 330 K, Asp is zwitterionic. The Asp/Cu(100) decomposition mechanism involves initial cleavage of the C3–C4 bond which occurs with the kinetics of a vacancy-mediated explosion. This step is followed by cleavage of the C1–C2 bond and the formation of a CH(NH₂)CH₂ intermediate that decomposes rapidly to yield N \equiv CCH₃ and H₂ in the gas phase. Using deuterated and ¹⁵N-labeled isotopomers of L-Asp, we demonstrate that scrambling of H(D) occurs during the decomposition of CH(NH₂)CH₂ into N \equiv CCH₃. The pre-exponential factors and activation energies of L-Asp decomposition on Cu(100) have been estimated from the decomposition kinetics using a rate law that consists of an initiation step and an explosion step.

ASSOCIATED CONTENT

S Supporting Information

The Supporting Information is available free of charge on the ACS Publications website at DOI: 10.1021/acs.langmuir.8b03482.

TPRS experiment results for L-Asp- 4^{-13} C, L-Asp- d_7 , L-Asp- $2,3,3-d_3$, and L-Asp- 1^5 N- $2,3,3-d_3$ decomposition with a constant heating rate of 0.5 K/s and at an isothermal temperature of 480 K (PDF)

AUTHOR INFORMATION

Corresponding Author

*E-mail: gellman@cmu.edu. Phone: 412-268-3848.

ORCID ®

Aaron Reinicker: 0000-0002-5297-5884 Andrew J. Gellman: 0000-0001-6618-7427

Note:

The authors declare no competing financial interest.

ACKNOWLEDGMENTS

This work has been funded by the US NSF under grant number NSF CHE 1764252.

REFERENCES

- (1) Baddeley, C. J.; Held, G. Chiral Molecules on Surfaces. *Comprehensive Nanoscience and Technology*; Elsevier, 2011; Vol. 3, pp 105–133.
- (2) Bada, J. L. Origins of homochirality. *Nature* **1995**, 374, 594–595.
- (3) Hazen, R. M.; Filley, T. R.; Goodfriend, G. A. Selective adsorption of L- and D-amino acids on calcite: Implications for biochemical homochirality. *Proc. Natl. Acad. Sci. U.S.A.* **2001**, 98, 5487–5490.
- (4) Smith, S. W. Chiral Toxicology: It's the Same Thing...Only Different. *Toxicol. Sci.* **2009**, *110*, 4–30.
- (5) Gellman, A. J. Chiral surfaces: accomplishments and challenges. *ACS Nano* **2010**, *4*, 5–10.
- (6) Horvath, J. D.; Koritnik, A.; Kamakoti, P.; Sholl, D. S.; Gellman, A. J. Enantioselective separation on a naturally chiral surface. *J. Am. Chem. Soc.* **2004**, *126*, 14988–14994.
- (7) Sholl, D. S.; Gellman, A. J. Developing chiral surfaces for enantioselective chemical processing. *AIChE J.* **2009**, *55*, 2484–2490.
- (8) Rampulla, D. M.; Gellman, A. J., Enantioselective decomposition of chiral alkyl bromides on Cu(6 4 3) R&S: Effects of moving the chiral center. **2006**; Vol. *600*, p 2823–2829. DOI: 10.1016/j.susc.2006.04.008
- (9) Yun, Y.; Kondratyuk, P.; Gellman, A. J. Steady-State Catalytic Decomposition of Aspartic Acid on Cu(111). *J. Phys. Chem. C* **2019**, DOI: 10.1021/acs.jpcc.8b01923.
- (10) Mhatre, B. S.; Dutta, S.; Reinicker, A.; Karagoz, B.; Gellman, A. J. Explosive enantiospecific decomposition of aspartic acid on Cu surfaces. *Chem. Commun.* **2016**, *52*, 14125–14128.
- (11) Gellman, A. J.; Huang, Y.; Koritnik, A. J.; Horvath, J. D. Structure-sensitive enantiospecific adsorption on naturally chiral Cu(hkl)^{R&S} surfaces. *J. Phys.: Condens. Matter* **2016**, *29*, 034001.
- (12) Gellman, A. J.; Huang, Y.; Feng, X.; Pushkarev, V. V.; Holsclaw, B.; Mhatre, B. S. Superenantioselective chiral surface explosions. *J. Am. Chem. Soc.* **2013**, *135*, 19208–19214.
- (13) Yun, Y.; Gellman, A. J. Enantioselective separation on naturally chiral metal surfaces: D,L-aspartic acid on Cu(3,1,17)^(R&S) surfaces. *Angew. Chem., Int. Ed.* **2013**, *52*, 3394–3397.
- (14) Yun, Y.; Gellman, A. J. Enantiospecific Adsorption of Amino Acids on Naturally Chiral Cu{3,1,17}^{R&S} Surfaces. *Langmuir* **2015**, *31*, 6055–6063.
- (15) Yun, Y.; Gellman, A. J. Adsorption-induced auto-amplification of enantiomeric excess on an achiral surface. *Nat. Chem.* **2015**, *7*, 520–525.
- (16) Totani, R.; Méthivier, C.; Cruguel, H.; Pradier, C.-M.; Humblot, V. Deciphering the Adsorption Mechanisms of RGD Subunits: L-Aspartic Acid on Cu(110). *J. Phys. Chem. C* **2017**, *121*, 15842–15850.
- (17) Costa, D.; Pradier, C.-M.; Tielens, F.; Savio, L. Adsorption and self-assembly of bio-organic molecules at model surfaces: A route towards increased complexity. *Surf. Sci. Rep.* **2015**, *70*, 449–553.
- (18) Yun, Y.; Wei, D.; Sholl, D. S.; Gellman, A. J. Equilibrium Adsorption of d- and l-Alanine Mixtures on Naturally Chiral Cu{3,1,17}^{R&S} Surfaces. *J. Phys. Chem. C* **2014**, *118*, 14957–14966.
- (19) Dutta, S.; Gellman, A. J. Enantiospecific Adsorption and Decomposition of D- and L-Asp Mixtures on Cu(643)^{R&S}. *Chimia Int. J. Chem.* **2018**, *72*, 404–410.
- (20) Mhatre, B. S.; Pushkarev, V.; Holsclaw, B.; Lawton, T. J.; Sykes, E. C. H.; Gellman, A. J. A Window on Surface Explosions: Tartaric Acid on Cu(110). *J. Phys. Chem. C* 2013, 117, 7577–7588.
- (21) Behzadi, B.; Romer, S.; Fasel, R.; Ernst, K.-H. Chiral Recognition in Surface Explosion. *J. Am. Chem. Soc.* **2004**, *126*, 9176–9177.
- (22) Falconer, J. L.; Madix, R. J. The kinetics and mechanism of the autocatalytic decomposition of HCOOH on clean Ni(110). *Surf. Sci.* 1974, 46, 473–504.
- (23) Falconer, J.; McCarty, J.; Madix, R. J. The Explosive Decomposition of Formic Acid on Clean Ni(110). *Jpn. J. Appl. Phys.* **1974**, *13*, 525.

(24) Mccarty, J.; Falconer, J.; Madix, R. J. Decomposition of formic acid on Ni(110) I. Flash decomposition from the clean surface and flash desorption of reaction products. *J. Catal.* **1973**, *30*, 235–249.

- (25) Lorenzo, M. O.; Humblot, V.; Murray, P.; Baddeley, C. J.; Haq, S.; Raval, R. Chemical Transformations, Molecular Transport, and Kinetic Barriers in Creating the Chiral Phase of (R, R)-Tartaric Acid on Cu(110). *J. Catal.* **2002**, 205, 123–134.
- (26) Méthivier, C.; Humblot, V.; Pradier, C.-M. l -Methionine adsorption on Cu(110), binding and geometry of the amino acid as a function of coverage. *Surf. Sci.* **2015**, *632*, 88–92.
- (27) Shavorskiy, A.; Eralp, T.; Schulte, K.; Bluhm, H.; Held, G. Surface chemistry of glycine on Pt{111} in different aqueous environments. *Surf. Sci.* **2013**, *607*, 10–19.
- (28) Stevens, J. S.; de Luca, A. C.; Pelendritis, M.; Terenghi, G.; Downes, S.; Schroeder, S. L. M. Quantitative analysis of complex amino acids and RGD peptides by X-ray photoelectron spectroscopy (XPS). Surf. Interface Anal. 2013, 45, 1238–1246.
- (29) Marti, E. M.; Methivier, C.; Pradier, C. M. (S)-Cysteine Chemisorption on Cu(110), from the Gas or Liquid Phase: An FT-RAIRS and XPS Study. *Langmuir* **2004**, *20*, 10223–10230.
- (30) Zubavichus, Y.; Fuchs, O.; Weinhardt, L.; Heske, C.; Umbach, E.; Denlinger, J. D.; Grunze, M. Soft X-ray-induced decomposition of amino acids: an XPS, mass spectrometry, and NEXAFS study. *Radiat. Res.* **2004**, *161*, 346–358.
- (31) Ihs, A.; Liedberg, B.; Uvdal, K.; Törnkvist, C.; Bodö, P.; Lundström, I. Infrared and photoelectron spectroscopy of amino acids on copper: Glycine, l-alanine and β -alanine. *J. Colloid Interface Sci.* **1990**, *140*, 192–206.
- (32) Kim, J. W.; Lee, Y. M.; Lee, S. M.; Son, M. J.; Kang, H.; Park, Y. Surface Reaction of Sulfur-Containing Amino Acids on Cu(110). *Langmuir* **2010**, *26*, 5632–5636.
- (33) Baldanza, S.; Cornish, A.; Nicklin, R. E. J.; Zheleva, Z. V.; Held, G. Surface chemistry of alanine on Cu{111}: Adsorption geometry and temperature dependence. *Surf. Sci.* **2014**, *629*, 114–122.
- (34) Uvdal, K.; Bodö, P.; Liedberg, B. l-cysteine adsorbed on gold and copper: An X-ray photoelectron spectroscopy study. *J. Colloid Interface Sci.* **1992**, *149*, 162–173.
- (35) Nicklin, R. E. J.; Cornish, A.; Shavorskiy, A.; Baldanza, S.; Schulte, K.; Liu, Z.; Bennett, R. A.; Held, G. Surface Chemistry of Alanine on Ni{111}. *J. Phys. Chem. C* 2015, 119, 26566–26574.
- (36) Löfgren, P.; Krozer, A.; Lausmaa, J.; Kasemo, B. Glycine on Pt(111): a TDS and XPS study. Surf. Sci. 1997, 370, 277–292.
- (37) Gardin, D. E.; Somorjai, G. A. Vibrational spectra and thermal decomposition of methylamine and ethylamine on nickel(111). *J. Phys. Chem.* **1992**, *96*, 9424–9431.
- (38) Waluyo, I.; Krooswyk, J. D.; Yin, J.; Ren, Y.; Trenary, M. Spectroscopic Identification of Surface Intermediates in the Dehydrogenation of Ethylamine on Pt(111). *J. Phys. Chem. C* **2013**, 117, 4666–4679.
- (39) Pearlstine, K. A.; Friend, C. M. Alteration in surface reaction selectivity of nitriles. 2. Acetonitrile on tungsten(100) and tungsten(100)-(5.times.1)-carbon. *J. Phys. Chem.* **1986**, 90, 4344–4347.
- (40) Huang, Y.; Sachtler, W. M. H. H/D exchange of amines and acetonitrile over transition metal catalysts. *J. Phys. Chem. B* **1998**, *102*, 6558–6565.
- (41) Mhatre, B. S. Super-Enantiospecific Autocatalytic Decomposition of Tartaric Acid and Aspartic Acid on Cu Surfaces, Ph.D. Thesis, Carnegie Mellon University, Pittsburgh, PA 2013.